Title: No unique scaling law for igneous dikes

Authors: S.P.A Gill[1], R.J. Walker[2,3*], K.J.W. McCaffrey[4], C. Greenfield[3]

Affiliations: [1]University of Leicester, School of Engineering, University Road, Leicester, LE1 7RH, UK. [2]Department of Earth and Planetary Sciences, University of California, Davis, 1 Shields Avenue, Davis, CA 95616, US. [3]University of Leicester, School of Geography, Geology, and the Environment, University Road, Leicester, LE1 7RH, UK. [4]Durham University, Department of Earth Sciences, Science Labs, South Road, Durham, DH1 3LE, UK.

*Corresponding author: rjwalker@ucdavis.edu
Author contacts:
spg3@leicester.ac.uk
k.j.w.mccaffrey@durham.ac.uk
cat.greenfield@leicester.ac.uk

Author twitter handles:
@DrRJWalker
@k_mccaffrey
@CatGreenfield

No unique scaling law for igneous dikes

S.P.A Gill[1], R.J. Walker[2,3], K.J.W. McCaffrey[4], C. Greenfield[3]

[1]University of Leicester, School of Engineering, University Road, Leicester, LE1 7RH, UK.

[2]Department of Earth and Planetary Sciences, University of California, Davis, 1 Shields Avenue, Davis, CA 95616, US

[3]University of Leicester, School of Geography, Geology, and the Environment, University Road, Leicester, LE1 7RH, UK

[4]Durham University, Department of Earth Sciences, Science Labs, South Road, Durham, DH1 3LE, UK.

Abstract

In linear elastic fracture mechanics (LEFM), veins, dikes, and sills grow in length when the stress intensity factor K_I at the tip reaches a critical value: the host rock fracture toughness K_{Ic}. This criterion is applied broadly in LEFM models for crack growth and assumes that the pressure inside the crack is uniform. When applied to intrusion length versus thickness scaling, a significant issue arises in that derived $K_{IC} = 300\ to\ 3000\ MPa\sqrt{m}$, which is about 100–1000 times that of measured K_{Ic} values for rocks at upper crustal depths. The same scaling relationships applied to comparatively short mineral vein data gives $K_{Ic} < 10\ MPa\sqrt{m}$, approaching the expected range. Here we propose that intrusions preserve non-equilibrated pressures as cracks controlled by kinetics, and therefore cannot be treated in continuum with fracture-controlled constant pressure (equilibrium) structures such as veins, or many types of scaled analogue model. Early stages of dike growth (inflation) give rise to increasing length and thickness, but magma pressure gradients within intrusions may serve to drive late-stage lengthening at the expense of maximum thickness (relaxation). For cracks in 2D, we find that intrusion scaling in non-equilibrium growth is controlled by the magma injection rate and initial dike scaling, effective (2D) host rock modulus, magma viscosity and cooling rate, which are different for all individual intrusions and sets of intrusions. A solidified intrusion can therefore achieve its final dimensions via many routes, with relaxation acting as a potentially significant factor, hence there is no unique scaling law for intrusions.

1. Introduction

A common method of characterising dike geometry is to plot their measured maximum thickness (T) against their horizontal length (L) (Fig. 1: see Schultz et al. (2008) and references therein). A similar method has been applied widely to fault systems to determine critical mechanical controls on intraplate fault evolution, in which the maximum displacement D_{max}

is related to L by $D_{max} = \gamma L^n$, where typically $n = 1$ (Cowie and Scholz, 1992; Schultz et al., 2008), with the difference being that D_{max} is a shear displacement whereas T is opening displacement. This exponent indicates a power law $D_{max} - L$ relationship (with scatter), which is inferred to represent scaling under constant stress loading (Scholz, 2008, 2019). For dikes and other opening mode fractures (e.g., joints, veins, and sills) $T– L$ scaling is typically shown as $n = 0.5$ (i.e. $T = \alpha\sqrt{L}$; Olson, 2003) albeit with significant scatter in aspect ratio at all data-rich length scales (Fig. 1A). In contrast to the frictional control for shear faults, this square root scaling would be consistent with growth under conditions of constant rock properties, including material fracture toughness K_{Ic} (Scholz, 2010); cracks would become unstable under constant stress loading, therefore implying growth under constant displacement boundary conditions (Segall, 1984). Understanding scaling relationships therefore has significant implications for the mechanics of intrusions and other opening mode fractures.

Opening displacement (thickness) versus length ($T– L$) data for dikes (and veins, sills, etc., but here we focus on dikes) are universally interpreted using a linear elastic 2D pressurised crack model. The model assumes mechanical equilibrium, such that the stress intensity, K_I, at the tip of the dike is equal to the mode I fracture toughness of the country rock, K_{Ic} (i.e., the ability of a material containing a crack to resist fracture). Magma flows within a conduit down a pressure gradient, so a static (equilibrium) condition necessarily requires that the magma pressure, P, is uniform within the dike, as shown in Fig. 1B. In reality, the ability of a magma to flow to relieve overpressure and achieve equilibrium will be directly dependent on magma viscosity, for which there is a significant range in nature (McLeod and Tait, 1999), rising sharply towards solidus temperatures. The failure condition at constant pressure is

$$K_I = P\sqrt{\frac{\pi L}{2}} = K_{Ic}. \tag{1}$$

The maximum thickness would be at the centre of this 2D dike and is given by

$$T = \frac{2}{E'} PL, \tag{2}$$

where $E' = \frac{E}{1-\nu^2}$ is the (2D) plane strain modulus of the country rock, E is the Young's modulus and ν is the Poisson's ratio. Combining Equations 1 and 2 gives the classic relationship between dike thickness and length (Olson, 2003)

$$T = \alpha L^{0.5}, \tag{3}$$

where the constant of proportionality is $\alpha = \sqrt{\frac{8}{\pi}}\frac{K_{Ic}}{E'}$. Figure 1A suggests that $10^{-2} < \alpha < 1\sqrt{m}$ encompasses the range of dikes observed in the field.

Measured thickness to length ratios are generally consistent with reasonable magma excess pressure estimates using Equation 2, in the range of 1–10 MPa (Rubin, 1995), but the large areas over which that pressure operates in a constant pressure model results in extremely large stress intensity at the tip, which then requires excessively large fracture toughness to stabilise the crack (Fig. 1A). It is widely acknowledged that this model-predicted value for fracture toughness is much larger than the expected values for the host rock (Rivalta et al., 2015; Cruden et al., 2017), with model results typically in the region of $K_{Ic} = 300 - 3000\ MPa\sqrt{m}$ on Earth (Schultz et al., 2008), with estimates up to $K_{Ic} = 15{,}000\ MPa\sqrt{m}$ on Mars (Rivas-Dorado et al., 2021); these predictions are compared to ~1 $MPa\sqrt{m}$ in nature (Atkinson, 1984). To appreciate how unphysical these calculated values are, the fracture toughness of all classes of material are shown in Figure 1C, where $\alpha \approx 10^{-5}\sqrt{m}$ for technical ceramics including glass, and $\alpha \approx 10^{-4}\sqrt{m}$ for building materials such as concrete and brick, with the very highest values of $\alpha \approx 10^{-3}\sqrt{m}$ for high-performance structural materials such as metal alloys. Predicted dike-model values of K_{Ic} are 2–3 orders of magnitude above the expected and measured range for rocks, and significantly above the toughest known materials, such as maraging steel (175 $MPa\sqrt{m}$) and titanium alloys (up to 107 $MPa\sqrt{m}$). Measured K_{Ic} for upper crustal rocks (0–5 km) ranges from about $0.5 - 3\ MPa\sqrt{m}$ (Stoeckhert et al., 2015), hence the equilibrium model of Equation 1 cannot explain what is physically observed using realistic material parameters. This problem is compounded given that the fracture toughness of brittle materials should reduce with length scale, due to the increased probability of encountering larger and larger pre-existing defects, from micro-cracks up to faults (Schultz 1993). The high toughness of metals shown in Figure 1C is due to their plasticity, and it could be argued that rock plasticity and/or increasing depth/temperature should increase K_{Ic} (Heimpel and Olson, 1994; Balme et al., 2004; Stoeckhert et al., 2015), but this is not enough to span the expectation gap, especially at the shallow crustal emplacement depths of the dikes plotted in Figure 1A. The GPa-scale values calculated for K_{Ic} are for already-long intrusions, which is particularly problematic in that the stress intensity is proportional to the crack length

(Equation 1), hence longer intrusions should be easier to grow than short intrusions; the model effectively predicts that it is impossible to grow a short intrusion since $K_I \ll K_{Ic}$ at shorter length scales. Any alternative model must therefore predict a stress intensity at the dike tip that is within a realistic fracture toughness range for rocks in the upper crust—on the order of $K_{Ic} \approx 1\ MPa\sqrt{m}$—which is the purpose of this paper. However, the existing toughness-controlled growth model would appear to be inappropriate. As an illustration, taking a typical dike from Figure 1 with $T = 6m$ and $L = 1\ km$, the equilibrium model predicts that a host rock with $K_{Ic} \approx 1000\ MPa\sqrt{m}$ is required to sustain this dike. If we keep the magma volume (area in the 2D case) constant, and reduce the fracture toughness to $K_{Ic} \approx 1\ MPa\sqrt{m}$ then Equation 3 predicts that this dike would have dimensions of $T = 6\ cm$ and $L = 100\ km$ at equilibrium. This shape is never likely to be achieved of course, since magma flow would cease due to solidification, and the final dike would be one that is frozen into a non-equilibrium state.

Here we revisit the assumptions of dike scaling laws, reapplying principles of kinetic (viscous) and fracture controls on crack growth. We find that dikes and veins do not occupy the same $T - L$ scaling continuum because of the fundamental controls on their growth and preservation in the rock record. Furthermore, the conditions of individual dike systems are sufficiently variable that no two systems are likely to follow the same scaling trajectory.

2. Kinetic-dominated versus toughness-dominated growth

Equation 1 assumes the dike is in an equilibrium state when it solidifies, i.e. the fluid (magma) has had time to redistribute itself within the fracture to remove all pressure gradients. This *toughness-dominated* assumption is reasonable for low viscosity fluids in small fractures, since the short distances involved mean that fluid pressure can equilibrate quickly. However, as noted above, non-equilibrated fracture geometry results in the prediction of unphysically high fracture toughness, so it is necessary to look at alternative explanations. The principal variable in linear elasticity that has influence on K_I, and that can be changed, is the excess magma pressure distribution, $p(x)$, where $-\frac{L}{2} \leq x \leq \frac{L}{2}$ is the lateral distance from the centre of the dike. The exact pressure profile in the dike is represented analytically by a series expansion (Spence and Sharp, 1985) but can be illustrated in simpler terms using the approximate solution of Spence and Turcotte (1985). They introduced a linear variation in the pressure such that $p(x) = P + \Delta P \left|\frac{2x}{L}\right|$, where P is the pressure at the centre of the dike and $P + \Delta P$ is the pressure at the tip. A value of $\Delta P = -\frac{\pi}{2}P$ removed the stress intensity at the tip entirely, i.e. $K_I = 0$, resulting in a negative tip pressure of $-0.57P$, as shown in Supplementary Material. This is

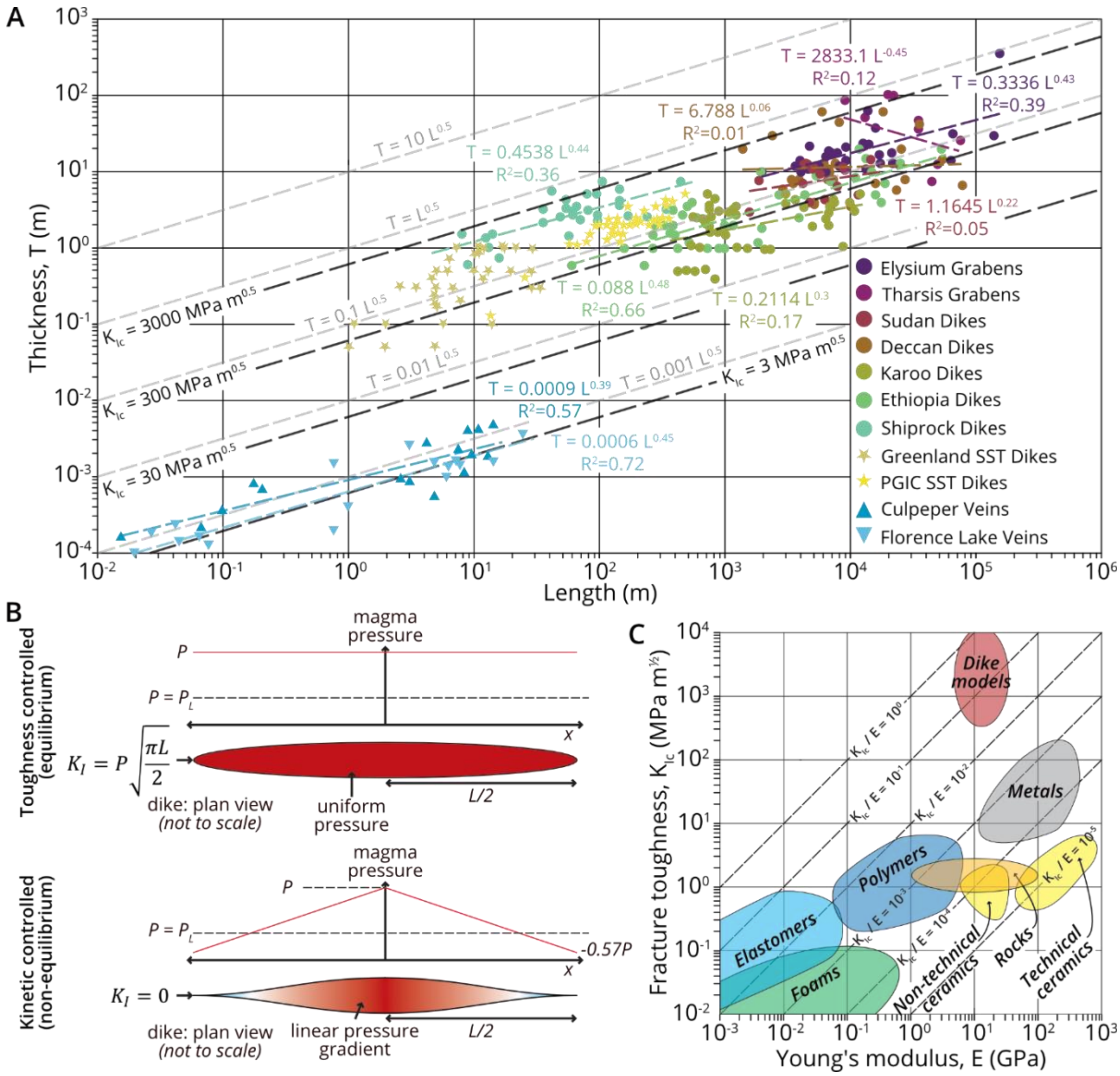

Figure 1: (A) Dike scaling relationship plot of maximum thickness (maximum opening displacement) versus length. Contours for fracture toughness K_{Ic} are from Cruden et al. (2017) and based on Young's Modulus $E = 100\ GPa$. Graben data (Rivas-Dorado et al., 2021) refers to dike dimensions, based on calculations using graben widths. Sudan, Deccan, Karoo, and Ethiopia, and Shiprock dike data are from Olson (2003) and Cruden et al. (2017), and Culpeper and Florence Lake vein data from Olson (2003). Sandstone (SST) dike data from Vétel and Cartwright (2010): PGIC, Panoche Giant Intrusion Complex (California, USA) **(B)** Pressure and dike thickness profiles for toughness-controlled (upper image) and kinetic-controlled (lower image) models, showing the mode I stress intensity at the dike tips, K_I, in both cases **(C)** Materials Selection Chart (adapted from Ashby, 2009) showing K_{IC} vs E for a range of materials. Note the position of K_{IC} values predicted from equilibrium-based intrusion scaling relationship models relative to the position occupied by natural rocks.

illustrated in the lower diagram in Figure 1B. For a pressure that continually decreases away from the centre, which is consistent with magma flowing toward the dike extremities, the excess pressure at the tip must always be negative for $K_I = 0$ (note, this is only a negative *excess* pressure, and once lithostatic pressure P_L is included, the total pressure is still positive and therefore compressive). This alternate extreme is referred to as *kinetic-dominated* behaviour, whereby a dike propagates in a non-equilibrium state determined by the rate at which magma is emplaced and redistributed within the fracture. It assumes that the fracture toughness is negligible compared to the large forces involved in dike propagation, such that it can be assumed that K_{Ic} is effectively zero. The primary assumption behind this model is that the crack tip must remain magma-filled, whereby any (low pressure) cavity that developed would quickly be filled or closed due to the large pressure difference between the magma or host rock and the cavity (Rubin, 1995). This model was first employed by Delaney and Pollard (1981), and it is generally accepted that the precise tip conditions in this respect are not that important (Rubin, 1995); e.g., the existence of tip cavities that are small compared to the dike length do not change the $K_{Ic} = 0$ assumption.

The kinetic-dominated versus toughness-dominated argument has been discussed in the literature for some time (see Rivalta et al, 2015). It is therefore useful to quantify the predicted $T - L$ scaling response where these regimes apply. To do this we utilise the simple 2D analytical approximation of Spence and Turcotte (1985), which allows for both finite toughness and finite viscosity, to model the growth of a (2D) dike with linearly increasing volume (area) $V_{2D} = Qt$, where Q is the injection rate (in units $m^2 s^{-1}$) as a function of time. Firstly, it is of particular interest to note that this allows us to obtain the same scaling relationship as Equation 3 (see Supplementary Material)

$$T = f(\lambda).\alpha L^{0.5} \tag{4}$$

but with a different constant of proportionality, where $f(\lambda)$ is a dimensionless scaling function which is a function of the dimensionless scaling parameter

$$\lambda = \left(\frac{L_K}{L_\eta}\right)^{\frac{1}{2}} = \frac{K_{Ic}}{(Q\eta E'^3)^{\frac{1}{4}}} \tag{5}$$

where $L_K = \left(\frac{K_{Ic}}{E'}\right)^2$ is the toughness-dominated length scale, and $L_\eta = \left(\frac{Q\eta}{E'}\right)^{\frac{1}{2}}$ is the kinetic-dominated length scale. In the latter, Q is the constant growth rate ($m^2 s^{-1}$) and η is magma viscosity ($Pa.s$). The parameter λ is the key measure of the balance between toughness-controlled ($\lambda \gg 1$) and kinetic-controlled ($\lambda \ll 1$) growth.

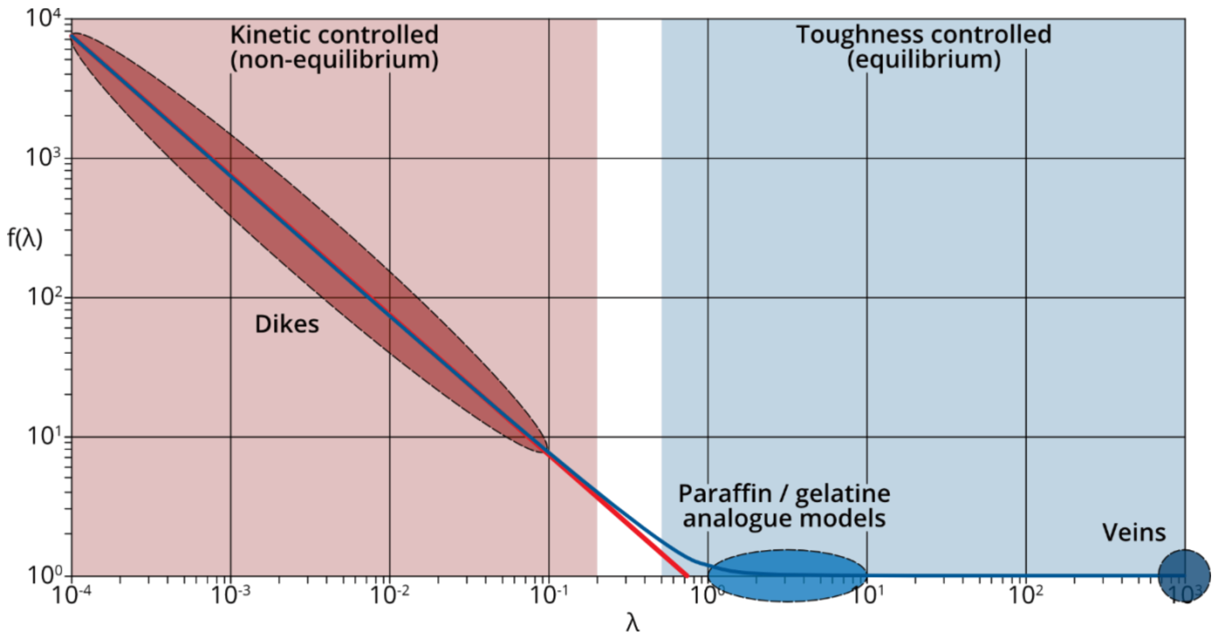

Figure 2. Plot of f versus λ. Thin blue line is the full solution (see Equation A.9 in Supplementary Materials). Thick red line is purely viscous model ($K_{Ic} = 0$) (see Equation A.10).

A plot of $f(\lambda)$ versus λ is shown as the blue line in Figure 2. It shows that $f = 1$ where toughness dominates, as expected from Equation 3, and that $f \gg 1$ where kinetic effects dominate. The red line shows the predictions for the purely kinetic regime ($K_{Ic} = 0$) for which

$$T = \left(\frac{6}{\pi}\right)^{\frac{1}{4}} \left(\frac{Q\eta}{E'}\right)^{\frac{1}{4}} L^{0.5} \tag{6}$$

in contrast to the toughness-dominated prediction of Equation 3. It is clear that systems are kinetics-dominated for $\lambda < 0.2$ and toughness-dominated for $\lambda > 0.4$ where $f = 1$. There is a small transition region in between, but it appears this is not significant enough to warrant a combined model; i.e., it is sufficient to use a toughness-dominated or a kinetics-dominated model. It is useful now to estimate where a particular system sits on this continuum, particularly when reflecting on the scaling relationships between laboratory models and natural fracture systems.

For dikes, if we assume $Q = 10^{-2} - 1\ m^2/s$, $\eta = 10^2 - 10^8\ Pa.s$, $K_{Ic} = 10^6\ Pa\sqrt{m}$ and $E' = 1 - 10\ GPa$, then we get $10^{-4} < \lambda < 10^{-1}$ (Fig. 2). Spence and Turcotte (1985) used lower viscosities and estimated $\lambda \approx 5 \times 10^{-3}$, but in any case, it is clear from Figure 2 that dikes are very strongly dominated by kinetics. Parameter λ can have a wide range of values, depending on the specific conditions under which a dike was emplaced, and predicts, therefore, a wide range of observed dike aspect ratios, consistent with the wide scatter in the observed data. This model suggests that rapid emplacement (large Q) of a viscous magma (large η) into a compliant host (low E') leads to the growth of a relatively short and thick dike (small λ and large f). The chosen viscosity range is high for a basaltic magma (typically taken as $\eta = 10^2\ Pa.s$), but in line with phenocryst-rich andesite or rhyolite magmas (Takeuchi, 2011 and references therein). Viscosity is a strong function of temperature, hence the viscosity of even basaltic magmas will approach such a high value as they approach solidus temperatures; a condition that becomes more likely towards the periphery of an intrusive system. In this model, low pressure gradients and slower plug-flows would reduce the effective channel width of the conduit, consistent with a higher viscosity.

In vein systems formed by hydrofracture (for purposes of comparison to Figure 1A, we are referring exclusively to syntaxial immobile vein systems; e.g., Bons et al., 2012), the viscosity of water at room temperature is $\eta = 10^{-3}\ Pa.s$ and much lower at higher temps. The final area (2D volume) is about $10^{-6} - 10^{-3}\ m^2$. The potential host lithologies are the same as for dikes, hence host rock fracture toughness and modulus are as above. Such a low viscosity fluid in a fracture of such small volume equilibrates almost instantly, and therefore it must be toughness-controlled. In large veins (>1 m aperture), complete sealing by mineral precipitation within the vein may occur very slowly or not at all (over years to millions of years; e.g., the calcite infills dated by Roberts and Walker, 2016) allowing ample time for the hydrofracture to relax towards equilibrium (if this was required). Hence veins are expected to be very strongly toughness-dominated ($\lambda \to \infty$).

In the context of kinetic versus toughness-controlled growth, it is also of interest to consider scaled analogue (laboratory) models, which each use different host materials and magma analogues. Here we focus on examples that aim to model dike ascent and materials that have measured values for fracture toughness: those that use a gelatin host analogue, typically with a low viscosity liquid (water or paraffin oil). For instance, using the constant flux experiments of Taisne and Tait (2011), the injection rate (which is in m^3/s so converted here to 2D by dividing by the dike width, which is roughly the same as the height) is $Q = 10^{-5}\ m^2/s$ and $\eta = 10^{-4} - 10^{-1}\ Pa.s$. The fracture toughness is not given, but can be determined from their Equation 7 and Figure 2 to be $K_{Ic} = 33\ Pa\sqrt{m}$, and $E' = 10^3\ Pa$. This gives $1 < \lambda < 10$. As with veins, this system is strongly toughness-dominated. Other analogue systems may fall outside of this range, such as those using granular mixtures (Schmeidel et al., 2017) or low-concentration laponite gels (Arachchige et al., 2021), and/or viscous fluids. The scaling mismatch in properties is noted elsewhere, in that for gelatine $\frac{K_{Ic}}{E'} = 10^{-2} - 10^{-1}$ (Kavanagh et al., 2013) whereas for rocks $\frac{K_{Ic}}{E'} = 10^{-4}$. This has the effect of increasing λ in those gelatine analogue models well into the fracture-controlled and equilibrium regime, and away from the region of natural dikes.

Taking $f = 1$ for veins in Figure 2 yields a prediction of $\alpha \approx 10^{-3}\sqrt{m}$ for the host rock in these cases. Host rock data determined from laboratory tests for the dike and vein systems in Figure 1A suggests that $\alpha \approx 10^{-4}\sqrt{m}$ in all cases. However, there is some evidence that modest increases in fracture toughness (by a factor of 3–5) could be possible at depth (Fialko and Rubin, 1997; Stoeckhert et al, 2016). Decreases in modulus are also possible at larger scales (Schultz, 1993) although this increase in compliance is largely due to the activity of joints which may be suppressed at depth. So we take $\alpha = 10^{-3}\sqrt{m}$ as the reference point. This is still consistent with the ranges assumed above, e.g. $K_{Ic} = 1\ MPa\sqrt{m}$ and $E' = 1\ GPa$. Plotting Equation 3 for values of $f(\lambda)$ on a thickness versus length diagram (Fig. 3), veins exist at about $f \approx 1$ and dikes are about $f = 10 - 1{,}000$. The exact results and position for dikes will therefore be dependent not only on the host rock properties, but also the magma flow rate and viscosity. Hence each dike system is unique and has the potential to occupy a different contour in $f(\lambda)$. This finding becomes apparent on closer inspection of individual datasets for dikes in Figure 1A. Although the data are very scattered, power law fits are plotted with the $n = 0.5$ exponent for all data (Olson, 2003). The Shiprock dikes ($n = 0.44$), Ethiopia dikes ($n = 0.48$) and Martian Elysium dikes ($n = 0.43$) each fit the $n = 0.5$ model of Equation 3 reasonably well. On the other hand, the Karoo dikes give $n = 0.3$, the Sudan dikes $n = 0.22$, and the Deccan dikes $n = 0.06$, potentially indicating different conditions of emplacement for each set. In any case, dikes, veins, and analogue models, are not part of the same continuum and cannot be linked in these thickness versus length scaling plots.

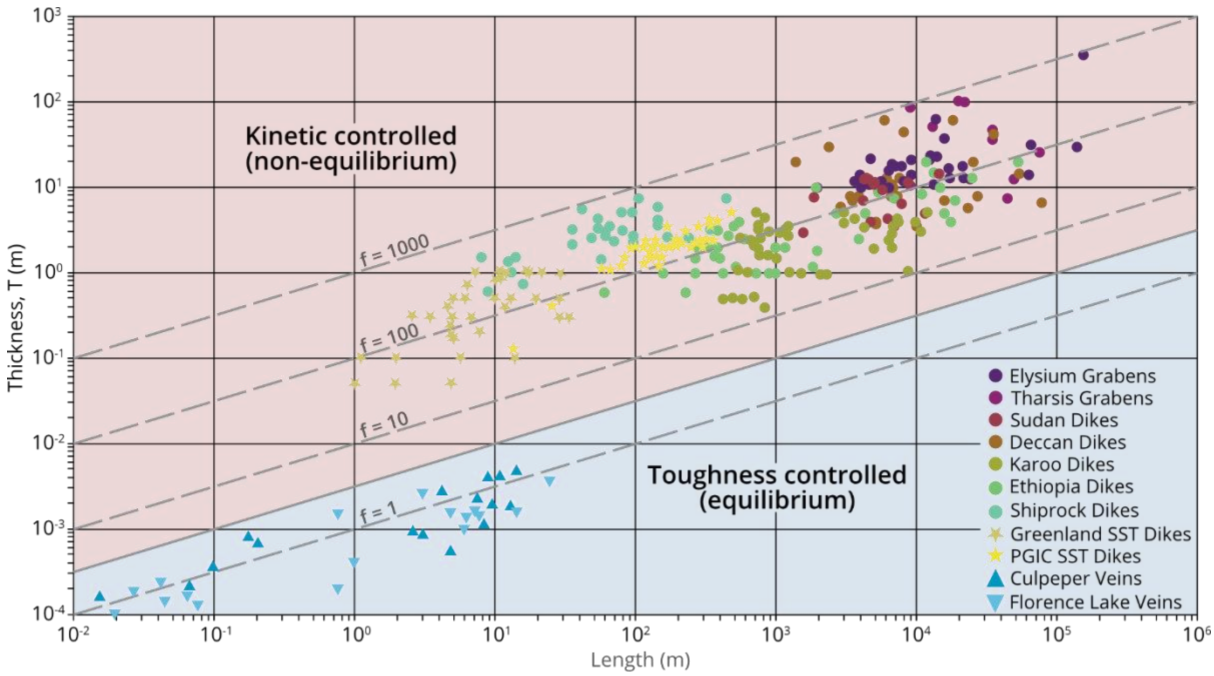

Figure 3. Interpretation of dike scaling observations using Equation (4) in terms of predicting toughness-dominated ($f = 1$) versus kinetic-dominated ($f > 1$) growth.

Before progressing further, it is useful to reflect on the importance of the 2D nature of the model presented. Savitski and Detournay (2002) developed a higher order 3D model for kinetic-dominated growth in a penny-shaped crack increasing in volume over time as $V_{3D} = qt$, where q is a constant with units of m^3/s. Taking the length to be the dike diameter, the scaling relationship, in this case

$$T = 3.0\left(\frac{q\eta}{E'}\right)^{\frac{1}{4}} L^{0.25} \tag{7}$$

gives a lower exponent of 0.25. However, this apparent conflict between the 2D and 3D models is easily resolved, as the final 2D model volume is $V_{2D} \approx \pi.\frac{TL}{4}$ and the final 3D model volume is $V_{3D} \approx \frac{4\pi}{3}.\frac{TL^2}{8}$ meaning that $q = \frac{2}{3}LQ$, where L is the final length of the dike. Substituting this scaling relationship in Equation (7) reproduces Equation (6) but with a different pre-factor (2.7) for the different geometry. The change in pre-factor is of little consequence, but this does raise the question about whether the magma injection rate depends on the final length of the dike, i.e. by inference, the volume of magma emplaced. In part this would depend on whether the entire magma volume is available throughout dike growth, and/or how long q can be physically sustained through magma supply. This is a question that cannot easily be answered, as it depends on many factors, such as the size of the magma packet that feeds the dike and its rate of ascent. However, it does not seem unreasonable to envisage that a large dike ($L \approx 100\ km$) might be fed somewhat more rapidly than a small dike ($L \approx 10\ m$) due to the enormous difference in the quantity of magma involved. The model of a size-invariant magma line source (Q per metre) in this case appears to be more appropriate than a size-invariant point source (q). As the former is more consistent with observations than the latter, we will proceed to develop the 2D model further, whilst noting that the 3D scaling can be obtained with the substitution of $q = \frac{2}{3}LQ$.

To summarise, the predictions of Figure 2 and the observations in Figures 1A and 3 both support the conclusion that dikes grow as non-equilibrium structures in the kinetic-dominated regime. Therefore, we now assume $K_{Ic} = 0$ for the remainder of this paper. When considering non-equilibrium growth we propose that a dike extends in two phases: (1) an *inflation* phase, where the volume of magma in the dike increases over time; followed by (2) a *relaxation* phase, where the magma volume is fixed but the dike continues to extend, accommodated by magma flow, until it freezes. It is of interest to determine whether relaxation plays a significant role in dike scaling, but also to check that a dike cannot reach equilibrium within the predicted relaxation time. A similar model has been proposed previously for progression of horizontal sheet intrusions in $T - L$ space, from (thick-short) laccolith to (thin-long) sill geometries (Bunger and Cruden, 2011) driven by magma body forces (the weight of the magma), but this does not apply in dikes.

3. Models for non-equilibrium inflation and relaxation phases

In the context of the observed order of magnitude variation in the scaling relationship observations of Figure 1A, here we wish to develop a simple analytical solution which is a reasonable approximation of the full solution. The work of Spence and Turcotte (1985) provides a good starting point for this. The novelty of the approach here is to extend their previous analysis for kinetics-dominated growth to allow a general expression for the volume evolution, $V_{2D}(t)$, such that non-linear inflation and relaxation can be considered, as illustrated in Figures 4 and 5. To model *inflation*, we assume power law growth with exponent s, such that $V_{2D}(t) = Qt^s$ (Fig. 4), then the $T - L$ relationship of Equation 6 can now be written in a more general form (see Supplementary Material) as

$$T = \left(\frac{6}{\pi}\right)^{\frac{1-m}{2}} \left(\frac{(3s+1)Q\eta}{4E'}\right)^{\frac{1+m}{6}} L^m \tag{8}$$

where $m = \frac{3\alpha-1}{3\alpha+1}$. Note that the exponent reduces to $m = \frac{1}{2}$ when $s = 1$ and Equation 6 is recovered.

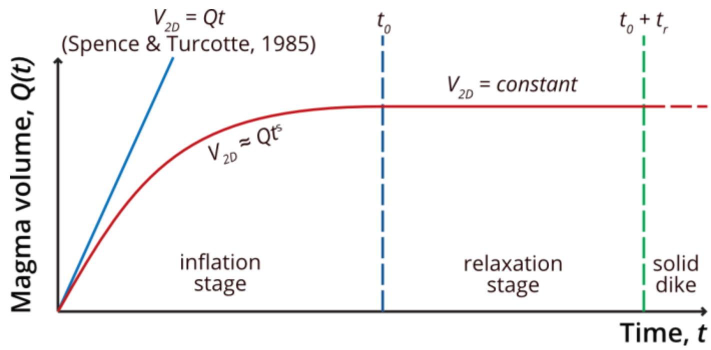

Figure 4. Schematic illustration of linear dike growth (e.g., Spence and Turcotte, 1985) in the which the 2D volume (area) relates to the injection rate, Q, as a function of time, t, relative to a non-linear magma injection model that uses a power law for the inflation stage up to time t_0, followed by an additional—constant volume—relaxation period of t_r before the dike solidifies.

To model the relaxation stage, we assume volumetric inflation ends at time $t = t_0$ with a final magma volume of $V_{2D}(t_0) = V_0 = Qt_0^s$. The dike can still evolve over time even without the addition of further magma, just at a much-reduced rate. If this evolution occurs for an additional relaxation time t_r then the total time is $t = t_0 + t_r$. In the Supplementary Material we find that during inflation the length increases as $t^{\frac{1}{6}+\frac{s}{2}}$ and during relaxation the length still increases but more slowly, tending towards $t^{\frac{1}{6}}$ when $t_r \gg t_0$. Similarly, the thickness increases during inflation as $t^{-\frac{1}{6}+\frac{s}{2}}$ and decreases during relaxation, tending towards $t^{-\frac{1}{6}}$ when $t_r \gg t_0$. As such, lengthening due to relaxation occurs at its fastest immediately following inflation, and will slow rapidly (e.g., Fig. 5). Even without accounting for the effect of cooling on viscosity, this means that a dike will not have sufficient time to reach equilibrium before it solidifies.

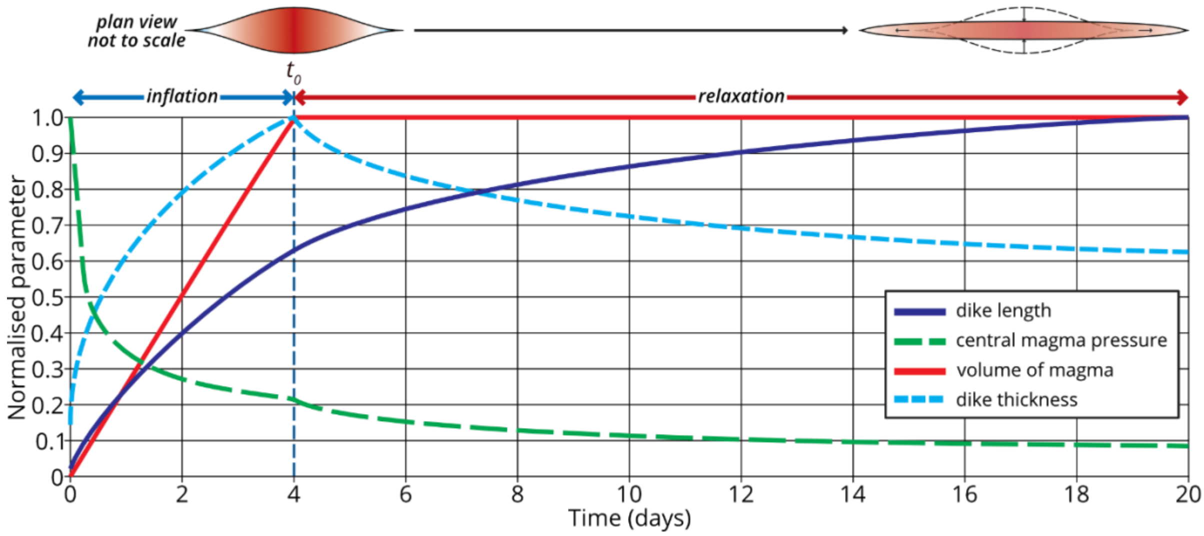

Figure 5. An example inflation-relaxation sequence, showing the temporal evolution of dike length, L, dike thickness, T, dike pressure, P, whereby a short, thick dike is rapidly injected over 4 days with an exponent of $s = 1$, leading to an increase in both its maximum (central) thickness and its length. At the end of the inflation phase, t_0, the dike relaxes the magma pressure over the following 16 days (t_r) by a further increase in length, necessarily accommodated by a decrease in dike maximum thickness to conserve magma volume.

To estimate the relaxation time, we use the widely adopted model of Turcotte and Schubert (2002) for solidification of a dike:

$$t_r = \frac{T^2}{16\kappa\beta^2} \tag{9}$$

where β is the Stefan constant and κ is the thermal diffusivity. Morita et al. (2006) calculated a value of $\beta = 0.36$ and $\kappa = 10^{-6}\ m^2 s^{-1}$. This predicts a 1 m thick dyke will take roughly 5.5 days to solidify, whereas a 5 m thick dyke would take 140 days. We now have two different time scales: (1) inflation during magmatic volume increase (t_0); and (2) relaxation during constant magmatic volume (t_r). As the dike thickness reduces during relaxation, such that $T(t_r)$, Equation (9) represent a quartic equation in terms of t_r (see Equation C.2 in Supplementary Material).

4. Theory vs Observations

Figure 6 illustrates a number of different dike growth and relaxation trajectories in $T - L$ space. In Figure 6A we follow the observations of Morita et al. (2006) and take a magma injection rate $Q = 1$, injection rate exponent $s = 0.65$, plane strain modulus $E' = 10\ GPa$, magma viscosity $\eta = 10^8\ Pa.s$, and thermal diffusivity $\kappa = 10^{-6}\ m^2/s$. The blue line in Figure 6A, and subsequent plots, shows the inflation trajectory, with points along it showing the dike dimensions after different growth periods. For $s = 0.65$ this has an exponent (slope) of $m = 0.33$. Once a dike stops increasing in volume, it progresses downward and to the right (increasing L at the expense of T) along its relaxation trajectory (the dashed lines connecting points). This terminates in the green line, which signifies the end of the solidification time predicted by Equation (9). The green line represents an upper bound on the relaxation time, as it does not take into account cooling during growth, or any increase in viscosity during relaxation, though again it is noted that relaxation will be fastest when it starts. The full extent of relaxation is therefore hard to determine, but it is expected that a dike of a given volume will form somewhere between the blue line and the green line. In Figure 6A, it can be seen that these conditions envelop a significant portion of the observed dikes. A dike reaches the first point (a length of 59 m and a thickness of 2.8 m) in 20 minutes. The upper bound on its relaxation time is then about 4 days, substantially longer than the growth time. In this case, neglecting cooling during inflation is reasonable. As dikes get larger, the inflation time increases relative to the relaxation time, as the thickness is not increasing as rapidly as the volume. For the dike observed in Morita et al. (2006) inflation takes 8 days but relaxation could be as long as 100 days thereafter. The very largest dike shown in Figure 6A grows to a length of 63 km over 40 years, but with only a comparatively short 8 years to relax. In this case, neglecting cooling during inflation is not reasonable, but as the amount of relaxation undertaken is insignificant this is not important. The relaxation curve always has a higher exponent (slope) than the inflation line, and in this case the exponent increases to 0.55 for the smallest dikes, converging back to 0.33 for the largest dikes. Figure 6B shows that reducing the viscosity to $\eta = 10^6\ Pa.s$ drops the inflation and relaxation curves downwards, towards some of the thinner dike sets. In Figure 6C, a higher magma injection rate of $Q = 10\ m^2 s^{-0.65}$ moves the growth curve upwards to encompass some of the thicker observed dikes, showing that the effect of relaxation could be quite substantial even in the larger length scales under this scenario. Figure 6D models rapid linear ($s = 1$) growth, for which nearly all the observed dikes sit between the inflation and relaxation curves. Figure 6E shows the effect of using a much lower exponent of $s = 0.5$ which now shows the effects of slower inflation, i.e. insignificant relaxation for large dikes. Finally, Figure 6F shows that decreasing the thermal diffusivity to $\kappa = 10^{-7}\ m^2/s$ leads to slower cooling and a wider zone between the inflation and relaxation curves as would be expected. Conversely, an increase in the thermal diffusivity will lead to a reduction in the zone of possibility for observed dikes.

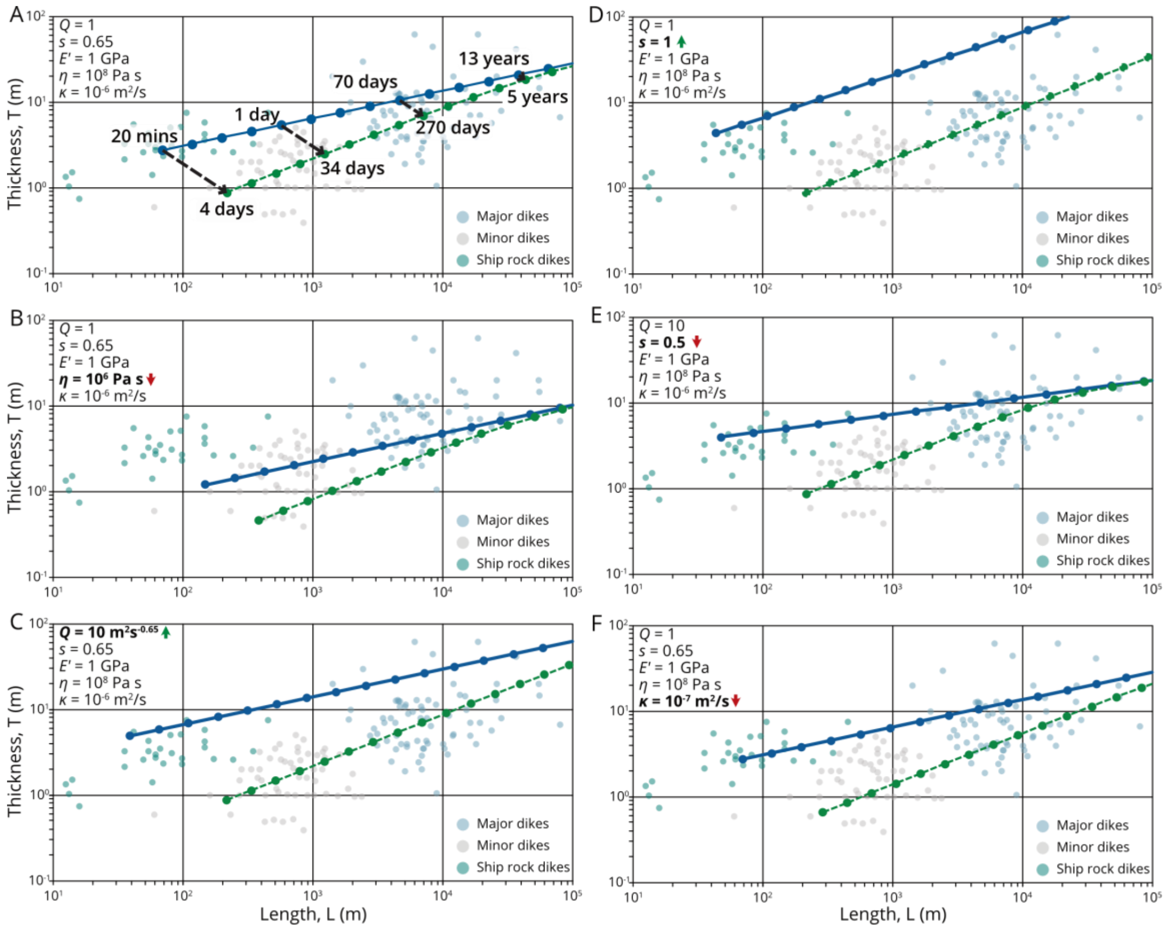

Figure. 6. Dike inflation and relaxation plots for different parameters: **(A)** $Q = 1$, $s = 0.65$, $E' = 1\,GPa$, $\mu = 10^8\ Pa.s$ and $\kappa = 10^{-6}\ m^2/s$. Plots in B–F show effects of changing individual parameters relative to (A), with: **(B)** reduced $\mu = 10^6\ Pa.s$; **(C)** higher growth rate $Q = 10\ m^2 s^{-0.65}$; **(D)** higher growth exponent (and rate) with $Q = 1$ and $s = 1$; **(E)** lower growth exponent $s = 0.5$ with increased $Q = 10$ (note that without increasing Q, growth takes hundreds of years); **(F)** lower thermal diffusivity (which affects cooling rate) with $\kappa = 10^{-7} m^2/s$. Observed dikes are expected to lie in the region between the upper (solid blue) and lower (dashed green) lines under the stated conditions. The Shiprock dikes are shown separately here as they are individual echelon surface segments of a larger underlying dike (Scholz, 2010) and hence are not necessarily expected to comply with the model presented here.

5. Comparison with natural intrusions

In our model, dikes can extend their length in two stages: (1) an inflation stage in which both length and thickness increase, and (2) a constant volume relaxation stage, in which length can only grow at the expense of maximum thickness. In reality the relaxation stage is likely to be highly variable, and dependent on the details of the cooling and solidification processes. The model shown here assumes that cooling initiates at the onset of the second stage, whereas for major dikes it is much more likely that parts will cool during the initial stage of volume increase, due to contact conduction with the host rock walls. The temperature distribution within the magma will therefore be a minimum at the walls and increase to a maximum at the centre. The picture is further complicated by the potential for temperature gain through the latent heat of crystallisation, and the increase in magma viscosity with crystal content. Here it is assumed that dike relaxation stops once it has solidified in the middle, at the position of maximum thickness, but this is not necessarily the case. Solidification within intrusions can be unevenly distributed, leading to localisation of magma flow into channels (e.g., Holness and Humphreys, 2003). This localised flow of hot magma can lead to remobilisation of accreted materials of variable viscosity across the conduit (e.g., Walker et al., 2017). Towards the tips, where the dike is much thinner, freezing could occur more rapidly. If the dike length is still extending at a sufficient rate (Delaney and Pollard, 1981) the magma at the tip will continue to be refreshed by an influx of hot material, preventing freezing. As such, the exact criteria that determines when a dike stops lengthening requires further investigation. The relaxation trajectories for length and thickness evolution shown as dashed green lines in Figure 6 therefore represent the maximum bound for relaxation. In nature then, some intermediary position of relaxation is probable, since a dike will undergo cooling during ascent, reheating as the magma crystallises, and further cooling to an ambient geotherm, set within host rocks and accreted dike margins that have variable thermal diffusivity properties. Relaxation presents, therefore, an additional process that will result in $T-L$ scatter for individual dikes within a larger volcanic system. The history of the freezing process will also determine the final internal pressure distribution, which will not be uniform or linear. This will be expressed in the final shape of the intrusion, which could result in a form between that of a lenticular geometry with tapered tip profiles, and the elliptical to superelliptical profiles associated with an equilibrium pressure distribution shown in Figure 1B (Spence and Turcotte, 1985; see e.g., the schematic illustrations in Fig. 5). This change in shape at the tip due to local magma redistribution in the final stages of freezing may change the stress distribution and failure mechanism at the tip (Walker et al., 2021; Stephens et al., 2021), which may affect intrusion lengthening, thereby introducing further scatter in $T-L$ space.

The question remains whether relaxation is evident during active intrusion and within the rock record. In active systems, Morita et al. (2006) provide some evidence for two stage growth in their study of earthquake swarms during dike intrusion in Izu Peninsula, Japan. From geodetic observations, they show that volume increase during dike growth occurred over 14 days, whereas associated seismicity occurred for 20 days. Based on their dimensions, the relaxation model here would have a conservative prediction for relaxation on the order of 100 days (maximum 400 days), which is far in excess of the six days indicated in the Morita et al. (2006) study. There are two immediate explanations for the discrepancy: (1) our model is an overestimate because there is likely to be significant cooling and potential solidification during the volumetric growth of the dike; and (2) fracture growth to accommodate relaxation may fall below seismicity detection limits (i.e., it becomes aseismic), particularly if growth is accommodated by dominantly tensile failure in the host rock (i.e., non-double couple mechanisms) as opposed to the shear-fracturing (double-couple mechanisms) shown in most dike seismicity studies. The latter explanation appears to be the case even for the volumetric inflation stages elsewhere, such as the Bárðabunga–Holuhran diking event in Iceland (Sigmundsson et al., 2015). Emplacement of the Bárðabunga–Holuhran dike induced earthquakes during growth laterally and towards the surface for about two weeks (Ágústsdóttir et al., 2016), followed by a six-month eruption phase, and a further six months of post eruption seismicity along the length of the dike section (Woods et al., 2019). Ágústsdóttir et al. (2016) interpret post-eruption earthquakes detected at 5–7 km depth as representing late-stage equilibration of magma pressure in the dike; i.e. relaxation. Geodetic measurements indicate that seismicity did not capture all pre-eruptive dike growth at shallow depths, including that necessary for magma to reach the surface (Sigmundsson et al., 2015), hence it is conceivable that some late stage growth may also go undetected in the shallow crust, particularly where dike lengthening is accommodated by tensile failure of the host rock (Rubin et al., 1998; Ágústsdóttir et al., 2016) or by dilatation of existing structures (Taisne et al., 2011). In any case, it is worth noting that eruption will have served to reduce excess magma pressure in the remaining dike, in which case the actual period of relaxation should be greatly reduced compared to the timescales predicted in Figure 6. In addition, the formation of a graben above the dike would likely place further constraints on the dike's ability to relax, as thickness reduction could require reactivation, and potentially inversion, of the graben fault system.

Lengthening during the relaxation stage may be a cryptic feature in the rock record also, since the diagnostic feature of relaxation is lengthening without volume increase, requiring thinning at some position along the dike (e.g., Daniels et al., 2012). Field-based studies of frozen intrusions have shown the potential for late-stage lengthening at preserved tip zones, that can be identified from overprinting textures and tip zone deformations (Stephens et al., 2021; Walker et al., 2021). The tip forms of such intrusions are typically blunted, with squared-ends and a relatively constant thickness compared to the bladed geometry that should result from rock splitting. In a linear elastic framework, this constant thickness would represent a constant magma pressure. However, such examples are commonly associated with distributed shear faulting at the tip, within the intruded host rock, which is interpreted to represent the magma front moving forward as a viscous indentor (Spacapan et al., 2017; Galland et al., 2019). This may still represent a constant pressure in the conduit, but could represent a plug flow of relatively cool and high viscosity magma. As noted above, introducing a plug flow regime is equivalent to changing the effective channel thickness in the model, and would therefore influence the relaxation model. Viscous indentation is also a relatively inefficient growth mechanism, particularly compared to elastic (tensile) splitting of the host rock, since the newly created fracture surfaces remain in contact and maintain a residual friction. Although a dike may grow by this mechanism over short distances, it is also possible that residual magma pressure may activate a new and more efficient pathway elsewhere on the dike (Walker et al., 2021), leading to only very local lengthening, and reducing the likelihood of observing the true maximum length dimension of the dike. In any case, these features are not necessarily uniquely related to a relaxation stage of growth, and further study would be required to constrain the distribution of such features at the periphery of individual dikes relative to changes in the thickness.

6. Conclusions

Toughness-dominated models for dike growth predict unreasonably large values for the rock fracture toughness, based on the assumption that magma pressure is constant within the dike, despite the need for pressure gradients to drive magma flow. Here we apply a kinetic-dominated analytical approach to consider the evolution of 2D dike geometry. Dike growth can be split into two stages, with a volume growth inflation stage characterised by lengthening and thickening, followed by a relaxation stage in which pressure gradients are relieved within the dike, leading to lengthening at the expense of maximum thickness. By changing the controlling parameters within a reasonable natural range, we find that the final length to thickness ratio for dikes can be achieved through multiple routes, rather than a unique power law relationship.

References

Ágústsdóttir, T., Woods, J., Greenfield, T., Green, R.G., White, R.S., Winder, T., Brandsdóttir, B., Steinthórsson, S. and Soosalu, H., 2016. Strike-slip faulting during the 2014 Bárðarbunga-Holuhraun dike intrusion, central Iceland. *Geophysical Research Letters*, *43*(4), pp.1495-1503.

Arachchige, U.N., Cruden, A.R. and Weinberg, R., 2021. Laponite gels-visco-elasto-plastic analogues for geological laboratory modelling. *Tectonophysics*, *805*, p.228773.

Ashby, M., 2009. The ces edupack resource booklet 2: Material and process charts. *Cambridge University, Cambridge, UK*.

Atkinson, B.K., 1984. Subcritical crack growth in geological materials. *Journal of Geophysical Research: Solid Earth*, *89*(B6), pp.4077-4114.

Balme, M.R., Rocchi, V., Jones, C., Sammonds, P.R., Meredith, P.G. and Boon, S., 2004. Fracture toughness measurements on igneous rocks using a high-pressure, high-temperature rock fracture mechanics cell. *Journal of Volcanology and Geothermal Research*, *132*(2-3), pp.159-172.

Bons, P.D., Elburg, M.A. and Gomez-Rivas, E., 2012. A review of the formation of tectonic veins and their microstructures. *Journal of Structural Geology*, *43*, pp.33-62.

Bunger, A.P. and Cruden, A.R., 2011. Modeling the growth of laccoliths and large mafic sills: Role of magma body forces. *Journal of Geophysical Research: Solid Earth*, *116*(B2).

Cowie, P.A. and Scholz, C.H., 1992. Displacement-length scaling relationship for faults: data synthesis and discussion. *Journal of Structural Geology*, *14*(10), pp.1149-1156.

Cruden, A.R., McCaffrey, K.J. and Bunger, A.P., 2017. Geometric scaling of tabular igneous intrusions: Implications for emplacement and growth. In *Physical Geology of Shallow Magmatic Systems* (pp. 11-38). Springer, Cham.

Daniels, K.A., Kavanagh, J.L., Menand, T. and R. Stephen, J.S., 2012. The shapes of dikes: Evidence for the influence of cooling and inelastic deformation. *Bulletin*, *124*(7-8), pp.1102-1112.

Delaney, P.T. and Pollard, D.D., 1981. *Deformation of host rocks and flow of magma during growth of minette dikes and breccia-bearing intrusions near Ship Rock, New Mexico* (No. 1202). USGPO,.

Fialko, Y.A. and Rubin, A.M., 1997. Numerical simulation of high-pressure rock tensile fracture experiments: Evidence of an increase in fracture energy with pressure?. *Journal of Geophysical Research: Solid Earth*, *102*(B3), pp.5231-5242.

Galland, O., Spacapan, J.B., Rabbel, O., Mair, K., Soto, F.G., Eiken, T., Schiuma, M. and Leanza, H.A., 2019. Structure, emplacement mechanism and magma-flow significance of igneous fingers–Implications for sill emplacement in sedimentary basins. *Journal of Structural Geology*, *124*, pp.120-135.

Heimpel, M. and Olson, P., 1994. Buoyancy-driven fracture and magma transport through the lithosphere: models and experiments. In *International geophysics* (Vol. 57, pp. 223-240). Academic Press.

Holness, M.B. and Humphreys, M.C.S., 2003. The Traigh Bhàn na Sgùrra sill, Isle of Mull: Flow localization in a major magma conduit. *Journal of Petrology*, *44*(11), pp.1961-1976.

Kavanagh, J.L., Menand, T. and Daniels, K.A., 2013. Gelatine as a crustal analogue: Determining elastic properties for modelling magmatic intrusions. *Tectonophysics*, *582*, pp.101-111.

McLeod, P. and Tait, S., 1999. The growth of dykes from magma chambers. *Journal of volcanology and Geothermal Research*, *92*(3-4), pp.231-245.

Morita, Y., Nakao, S. and Hayashi, Y., 2006. A quantitative approach to the dike intrusion process inferred from a joint analysis of geodetic and seismological data for the 1998 earthquake swarm off the east coast of Izu Peninsula, central Japan. *Journal of Geophysical Research: Solid Earth*, *111*(B6).

Olson, J.E., 2003. Sublinear scaling of fracture aperture versus length: an exception or the rule?. *Journal of Geophysical Research: Solid Earth*, *108*(B9).

Rivalta, E., Taisne, B., Bunger, A.P. and Katz, R.F., 2015. A review of mechanical models of dike propagation: Schools of thought, results and future directions. *Tectonophysics*, *638*, pp.1-42.

Rivas-Dorado, S., Ruiz, J. and Romeo, I., 2021. Subsurface Geometry and Emplacement Conditions of a Giant Dike System in Elysium Fossae, Mars. *Journal of Geophysical Research: Planets*, *126*(1), p.e2020JE006512.

Roberts, N.M. and Walker, R.J., 2016. U-Pb geochronology of calcite-mineralized faults: Absolute timing of rift-related fault events on the northeast Atlantic margin. *Geology*, *44*(7), pp.531-534.

Rubin, A.M., 1995. Propagation of magma-filled cracks. *Annual Review of Earth and Planetary Sciences*, *23*(1), pp.287-336.

Rubin, A.M., Gillard, D. and Got, J.L., 1998. A reinterpretation of seismicity associated with the January 1983 dike intrusion at Kilauea Volcano, Hawaii. *Journal of Geophysical Research: Solid Earth*, *103*(B5), pp.10003-10015.

Savitski, A.A. and Detournay, E., 2002. Propagation of a penny-shaped fluid-driven fracture in an impermeable rock: asymptotic solutions. *International journal of solids and structures*, *39*(26), pp.6311-6337.

Schmiedel, T., Galland, O. and Breitkreuz, C., 2017. Dynamics of sill and laccolith emplacement in the brittle crust: role of host rock strength and deformation mode. *Journal of Geophysical Research: Solid Earth*, *122*(11), pp.8860-8871.

Scholz, C.H., 2010. A note on the scaling relations for opening mode fractures in rock. *Journal of Structural Geology*, *32*(10), pp.1485-1487.

Scholz, C.H., 2019. *The mechanics of earthquakes and faulting*. Cambridge University Press.

Schultz, R.A., 1993. Brittle strength of basaltic rock masses with applications to Venus. *Journal of Geophysical Research: Planets*, *98*(E6), pp.10883-10895.

Schultz, R.A., Soliva, R., Fossen, H., Okubo, C.H. and Reeves, D.M., 2008. Dependence of displacement–length scaling relations for fractures and deformation bands on the volumetric changes across them. *Journal of Structural Geology*, *30*(11), pp.1405-1411.

Segall, P., 1984. Formation and growth of extensional fracture sets. *Geological Society of America Bulletin*, *95*(4), pp.454-462.

Sigmundsson, F., Hooper, A., Hreinsdóttir, S., Vogfjörd, K.S., Ófeigsson, B.G., Heimisson, E.R., Dumont, S., Parks, M., Spaans, K., Gudmundsson, G.B. and Drouin, V., 2015. Segmented lateral dyke growth in a rifting event at Bárðarbunga volcanic system, Iceland. *Nature*, *517*(7533), pp.191-195.

Spacapan, J.B., Galland, O., Leanza, H.A. and Planke, S., 2017. Igneous sill and finger emplacement mechanism in shale-dominated formations: a field study at Cuesta del Chihuido, Neuquén Basin, Argentina. *Journal of the Geological Society*, *174*(3), pp.422-433.

Spence, D.A. and Sharp, P., 1985. Self-similar solutions for elastohydrodynamic cavity flow. *Proceedings of the Royal Society of London. A. Mathematical and Physical Sciences*, *400*(1819), pp.289-313.

Spence, D.A. and Turcotte, D.L., 1985. Magma-driven propagation of cracks. *Journal of Geophysical Research: Solid Earth*, *90*(B1), pp.575-580.

Stephens, T., Walker, R., Healy, D. and Bubeck, A., 2021. Segment tip geometry of sheet intrusions, II: Field observations of tip geometries and a model for evolving emplacement mechanisms. *Volcanica*, *4*(2), pp.203-225.

Stoeckhert, F., Brenne, S., Molenda, M. and Alber, M., 2016, August. Mode I fracture toughness of rock under confining pressure. In *ISRM international symposium-EUROCK 2016*. OnePetro.

Stoeckhert, F., Molenda, M., Brenne, S. and Alber, M., 2015. Fracture propagation in sandstone and slate–Laboratory experiments, acoustic emissions and fracture mechanics. *Journal of Rock Mechanics and Geotechnical Engineering*, *7*(3), pp.237-249.

Taisne, B., Tait, S. and Jaupart, C., 2011. Conditions for the arrest of a vertical propagating dyke. *Bulletin of Volcanology*, *73*(2), pp.191-204.

Takeuchi, S., 2011. Preeruptive magma viscosity: An important measure of magma eruptibility. *Journal of Geophysical Research: Solid Earth*, *116*(B10).

Turcotte, D.L. and Schubert, G., 2002. *Geodynamics*. Cambridge university press.

Vétel, W. and Cartwright, J., 2010. Emplacement mechanics of sandstone intrusions: insights from the Panoche Giant Injection Complex, California. *Basin Research*, *22*(5), pp.783-807.

Walker, R.J., Branney, M.J. and Norry, M.J., 2017. Dike propagation and magma flow in a glassy rhyolite dike: A structural and kinematic analysis. *Bulletin*, *129*(5-6), pp.594-606.

Walker, R., Stephens, T., Greenfield, C., Gill, S., Healy, D. and Poppe, S., 2021. Segment tip geometry of sheet intrusions, I: Theory and numerical models for the role of tip shape in controlling propagation pathways. *Volcanica*, *4*(2), pp.189-201.

Woods, J., Winder, T., White, R.S. and Brandsdóttir, B., 2019. Evolution of a lateral dike intrusion revealed by relatively-relocated dike-induced earthquakes: The 2014–15 Bárðarbunga–Holuhraun rifting event, Iceland. *Earth and Planetary Science Letters*, *506*, pp.53-63.

Supplementary material: No unique scaling law for igneous dikes

A. Kinetics-dominated versus toughness-dominated growth for linear pressure model

Spence and Turcotte (1985) developed a first-order approximate model for the growth of a 2D dike of length L and thickness T in a linear elastic host with plane strain modulus $E' = \frac{E}{1-\nu^2}$, fracture toughness K_{Ic}, and magma viscosity η. This analysis is re-evaluated here for the purposes of dike scaling interpretation, and to investigate the criteria for transition between toughness and kinetic-controlled dike formation.

Stress intensity at the dike tip

The mode I stress intensity at the tip of a crack of length $L = 2a$ subject to an internal pressure distribution $p(x)$ is given by

$$K_I = \frac{1}{\sqrt{\pi a}} \int_{-a}^{a} p(x) \sqrt{\frac{a+x}{a-x}} dx \tag{A.1}$$

A simple linear approximation to the pressure distribution is proposed such that $p(x) = P + \Delta P \left|\frac{x}{a}\right|$. In this case equation (A.1) gives

$$K_I = \sqrt{\frac{a}{\pi}} \left(\pi P + 2\Delta P\right) \tag{A.2}$$

The condition for fracture propagation is $K_I = K_{Ic}$. Given the central magma pressure P, it is then required that

$$\Delta P = \frac{\pi}{2}\left[\frac{K_{IC}}{\sqrt{\pi a}} - P\right] \tag{A.3}$$

for dike propagation to occur. In the kinetic-controlled limit we can assume that the material resistance of the host rock is negligible ($K_{Ic} = 0$) which yields the result that $\Delta P = -\frac{\pi}{2} P$.

Spence and Turcotte (1985) analysis

The volume (area) of the 2D dike is assumed to evolve as a prescribed function of time, $V = Qt$, where Q (m^2/s) is a constant, and the magma pressure is assumed to be linear, such that

$p(x) = P\left[1 - \frac{\pi}{2}\left|\frac{x}{a}\right|\right]$ as derived above. [Note the problem with the exact pressure distribution was solved numerically by Spence and Sharp (1985) for self-similar dike evolution with $V(t) = Qt^{\alpha}$, but here we pursue an analytical approximation]. From their analysis we have the following parameters from their equations (24) to (26)

$$\gamma = \frac{2K}{(6Q\eta E')^{\frac{1}{4}}} = \left(\frac{4}{3\pi}\right)^{\frac{1}{4}} \frac{(6A_0^3 - 1)}{(1 + 12A_0^3)^{\frac{3}{4}}}$$

$$k = \frac{(1 + 12A_0^3)^{\frac{1}{2}}}{\sqrt{12\pi}A_0^2}$$

$$K = \frac{K_{IC}}{\sqrt{\pi}} \tag{A.4}$$

such that the parameter introduced in our equation (5) is defined in terms of these as

$$\lambda = \frac{K_{Ic}}{(Q\eta E')^{\frac{1}{4}}} = \frac{6^{\frac{1}{4}}\sqrt{\pi}}{2}\gamma = \left(\frac{\pi}{2}\right)^{\frac{1}{4}} \frac{(6A_0^3 - 1)}{(1 + 12A_0^3)^{\frac{3}{4}}} \tag{A.5}$$

The dike length and thickness are given in terms of the parameters in (A.4) by equations (27) and (28) in Spence and Turcotte (1985)

$$L = \frac{2}{6^{\frac{1}{6}}}.kQ^{\frac{1}{2}}\left(\frac{E'}{\eta}\right)^{\frac{1}{6}} t^{\frac{2}{3}}$$

$$T = 2.6^{\frac{1}{6}}.kA_0.Q^{\frac{1}{2}}\left(\frac{\eta}{E'}\right)^{\frac{1}{6}} t^{\frac{1}{3}} \tag{A.6}$$

where t is time. These can be combined to give

$$T = 24^{\frac{1}{4}}k^{\frac{1}{2}}A_0\left(\frac{Q\eta}{E'}\right)^{\frac{1}{4}} L^{\frac{1}{2}} \tag{A.7}$$

Following equation (4) we write this as

$$T = f.\sqrt{\frac{8}{\pi}}\frac{K_{Ic}}{E'}L^{\frac{1}{2}}$$

(A.8)

such that

$$f = \sqrt{\frac{\pi}{8}}.24^{\frac{1}{4}}\frac{k^{\frac{1}{2}}A_0}{\lambda} = \frac{(1+12A_0^3)}{2(6A_0^3-1)}$$

(A.9)

This is the blue line shown in Figure 2.

Now, in the *kinetic-controlled limit* ($\lambda \to 0$) we have $\gamma \to 0$ so (A.1) gives $6A_0^3 = 1$ such that

$$f = \sqrt{\frac{3\pi}{32}}\lambda^{-1}$$

(A.10)

This is the red line shown in Figure 2 and shows that the kinetic-controlled limit is valid for $\lambda < 0.2$. Given 2D volume (area) $V_{2D} = Qt$ we can also write this as

$$L = \sqrt{\frac{6}{\pi}}\left(\frac{E'}{Q\eta}\right)^{\frac{1}{6}}V_{2D}^{\frac{2}{3}} = \sqrt{\frac{6}{\pi}}\left(\frac{V_{2D}^2}{L_\eta}\right)^{\frac{1}{3}} \qquad T = \sqrt{\frac{6}{\pi}}\left(\frac{Q\eta}{E'}\right)^{\frac{1}{6}}V_{2D}^{\frac{1}{3}} = \sqrt{\frac{6}{\pi}}\left(L_\eta V_{2D}\right)^{\frac{1}{3}}$$

(A.11)

and

$$T = \left(\frac{6}{\pi}\right)^{\frac{1}{4}}\left(L_\eta L\right)^{\frac{1}{2}}$$

(A.12)

which only depends on the kinetic length scale L_η as expected.

In the *toughness-controlled limit* ($\lambda \to \infty$) we note that equations (34) and (35) in Spence and Turcotte (1985) are wrong, as they show a η dependence which should not be there in this regime. Carrying out the algebraic substitutions correctly, the actual result is as follows. In the limit of $\lambda \to \infty$ we get

$$\lambda = \left(\frac{3\pi}{8}\right)^{\frac{1}{4}} A_0^{\frac{3}{4}} \qquad \text{(A.13)}$$

then

$$k = \left(\frac{3}{8\pi^2}\right)^{\frac{1}{6}} . \lambda^{-\frac{2}{3}} \qquad \text{(A.14)}$$

giving, from (A.6),

$$L = \left(\frac{2}{\pi}\right)^{\frac{1}{3}} \lambda^{-\frac{2}{3}} Q^{\frac{1}{2}} \left(\frac{E'}{\eta}\right)^{\frac{1}{6}} t^{\frac{2}{3}} = \left(\frac{2}{\pi}\right)^{\frac{1}{3}} \left(\frac{QE'}{K_{IC}}\right)^{\frac{2}{3}} t^{\frac{2}{3}} \qquad \text{(A.15)}$$

and

$$T = 2\left(\frac{2}{\pi}\right)^{\frac{2}{3}} \lambda^{\frac{2}{3}} Q^{\frac{1}{2}} \left(\frac{\eta}{E'}\right)^{\frac{1}{6}} t^{\frac{1}{3}} = 2\left(\frac{2}{\pi}\right)^{\frac{2}{3}} \left(\frac{Q^{\frac{1}{2}} K_{Ic}}{E'}\right)^{\frac{2}{3}} t^{\frac{1}{3}} \qquad \text{(A.16)}$$

Writing this in terms of $V_{2D} = Qt$ gives

$$L = \left(\frac{2}{\pi}\right)^{\frac{1}{3}} \left(\frac{E'}{K_{IC}}\right)^{\frac{2}{3}} V_{2D}^{\frac{2}{3}} = \left(\frac{2}{\pi}\right)^{\frac{1}{3}} \left(\frac{V_{2D}^2}{L_K}\right)^{\frac{1}{3}} \qquad T = 2\left(\frac{2}{\pi}\right)^{\frac{2}{3}} \left(\frac{K_{Ic}}{E'}\right)^{\frac{2}{3}} V_{2D}^{\frac{1}{3}} = 2\left(\frac{2}{\pi}\right)^{\frac{2}{3}} (L_K V_{2D})^{\frac{1}{3}} \qquad \text{(A.17)}$$

Combining these gives our equation (3)

$$T = \sqrt{\frac{8}{\pi}} (L_K L)^{\frac{1}{2}} = 1.60 (L_K L)^{\frac{1}{2}} \qquad \text{(A.18)}$$

which only depends on the toughness length scale as expected, and yields $f = 1$ in this case as required.

B. Non-linear inflation and relaxation model

The aim here is to extend the analysis of Spence and Turcotte (1985), which has been re-evaluated in appendix A, to be applicable to the general case where $V(t)$ is a general function of time. Here an approximate analytical solution is derived using a variational method for kinetic processes defined by Cocks et al. (1998). This postulates that the best estimate of a kinetic field minimises a variational functional

$$\Pi = \Psi + \dot{G} \tag{B.1}$$

where Ψ is a dissipation potential and $\dot{G}$ is the rate of change of Gibbs free energy. In this case, the dissipation is due to magma flow. The Gibbs free energy is the driving force for this flow. In general it has two contributions

$$G = U_e + 2\Gamma L \tag{B.2}$$

where U_e is the change in elastic strain energy in the host rock due to changes in the dike geometry and/or magma pressure (equivalent to the energy release rate for crack growth), and $2\Gamma L$ is the fracture energy, where $\Gamma \approx \frac{K_{Ic}^2}{2E'}$ is the (constant) energy per unit area of fracture and $2L$ is the area of the crack face created as two crack faces are produced by splitting. Here the analysis is limited to the kinetic-controlled regime such that the second term is omitted, i.e. $\Gamma = 0$.

Gibbs free energy, G

Here we utilise the fact that in linear elasticity the change in elastic strain energy, $U_e = \frac{1}{2}\Omega$, is half the work done by the applied load. Here, this is the work done by the internal pressure, $p(x)$, in generating an opening thickness, $h(x)$

$$\Omega = \int_{-a}^{a} p(x)h(x)dx \tag{B.3}$$

The deformed shape for the assumed kinetic-controlled pressure profile, written as $p(\xi) = P\left[1 - \frac{\pi}{2}\ |\xi|\right]$ is given by equation (20) in Spence and Turcotte (1985) as

$$h(\xi) = \frac{2PL}{E'}\left[\sqrt{1-\xi^2} + \frac{1}{2}\xi^2 \ln\left(\frac{1-\sqrt{1-\xi^2}}{1+\sqrt{1-\xi^2}}\right)\right] \tag{B.4}$$

where $\xi = x/a$. Note that the definition of maximum thickness, $T = h(0)$, recovers equation (2). The volume of the magma-filled crack is

$$V(t) = \frac{L}{2}\int_{-1}^{1} h(\xi)d\xi = 1.051\frac{PL^2}{E'} = 0.525\,LT \tag{B.5}$$

Evaluation of the integral (B.3) gives

$$\Omega = 0.527\frac{P^2L^2}{E'} = \tilde{\beta}PV \tag{B.6}$$

where $\tilde{\beta} = 0.502$. This scaling is universal, with only the exact value of the pre-factor $\tilde{\beta}$ depending on the choice of pressure distribution within the dike. Note that for a uniform pressure of $p(x) = P$ the pressure term can be moved out of the integral in (B.3) such that $\Omega = PV$ in this case. Hence it is expected that the actual distribution will produce a pre-factor somewhere between these two cases, i.e. $\tilde{\beta}$ is between 0.5 and 1.0.

Dissipation potential, Ψ

The average magma flux through the dike at a distance x from the centre assumes laminar flow such that magma flows down the pressure gradient

$$j(x) = -kf_p \tag{B.7}$$

where $k(x) = \frac{h(x)^3}{12\eta}$ is the permeability of the magma channel and $f_p = \frac{\partial p}{\partial x}$ is the driving force for flow per unit volume. Following Cocks et al. (1998) we write this in terms of a dissipation rate per unit volume ψ such that

$$f_p = -\frac{\partial \psi}{\partial j} \tag{B.8}$$

The total dissipation can then be determined from (B.7) and (B.8) to be

$$\Psi = \int_{-a}^{a} \psi dx = \frac{1}{2}\int_{-a}^{a} \frac{j^2}{k} dx \tag{B.9}$$

The flux is related to the dike shape. For $0 \leq x \leq a$ we have

$$j(x) = -\int_0^x \frac{\partial h}{\partial t} dx + j_0 \tag{B.10}$$

where the flux at the centre of the dike is $j(0) = j_0$. It is tempting to determine the flux using the dike profile defined by (B.4) for the linear pressure gradient, but this is not possible as the chosen pressure distribution is not an exact solution. In practice the pressure gradient f at the tip must be infinite to generate a finite flux where the dike thickness h is zero (Rubin, 1995). If (B.4) is used then the dissipation potential is infinite at the tip. To simply generate an estimate of the dissipation, we therefore assume a simple rectangular dike shape, whereby the dike is of length L and average thickness $\tilde{T}$ where volume conservation requires that $V = L\tilde{T}$. This will provide the correct scaling, and the contribution from the actual shape can be calibrated later from the solution of Spence and Turcotte (1985). Equation (B.5) yields the relation $\tilde{T} = cT$, where $c = 0.525$. Now (B.10) becomes

$$j(x) = -\int_0^x \frac{\partial \tilde{T}}{\partial t} dx + j_0 = -c\dot{T}x + j_0 \tag{B.11}$$

where $j_0 = \frac{1}{2}\dot{V} > 0$ is the rate of change of half the magma volume in the growing dike. Given $\dot{V} = c(\dot{T}L + T\dot{L})$ we can write this as

$$j(x) = cT\dot{a}\left(\frac{x}{a}\right) + j_0\left(1 - \frac{x}{a}\right) \tag{B.12}$$

To calculate (B.9) we assume an average permeability $\tilde{k} = d.\frac{\tilde{T}^3}{12\eta}$ where the pre-factor d is to be determined based on the dike shape. The dissipation potential is therefore

$$\Psi = \frac{L}{12\tilde{k}}\left[\left(cT\dot{L}\right)^2 + cT\dot{L}\dot{V} + \dot{V}^2\right] \tag{B.13}$$

Variational functional, Π

We write $P = \frac{E'T}{2L} = \frac{E'V}{2cL^2}$ from equation (2) such that (B.6) becomes $\Omega = \frac{\tilde{\beta}E'V^2}{2cL^2}$ and hence

$$\dot{G} = \frac{1}{2}\dot{\Omega} = \frac{\tilde{\beta}E'V^2}{2cL^2}\left[\frac{\dot{V}}{V} - \frac{\dot{L}}{L}\right] \tag{B.14}$$

The variational functional (B.1) can therefore be written as

$$\Pi = \frac{L}{12\tilde{k}}\left[\left(cT\dot{L}\right)^2 + cT\dot{L}\dot{V} + \dot{V}^2\right] + \frac{\tilde{\beta}E'V^2}{2cL^2}\left[\frac{\dot{V}}{V} - \frac{\dot{L}}{L}\right] \tag{B.15}$$

As $\dot{V}$ is prescribed in this analysis, the only kinetic degree-of-freedom is $\dot{L}$ whose optimal solution minimises (B.15) such that $\frac{\partial\Pi}{\partial\dot{L}} = 0$. This gives

$$\frac{L}{12\tilde{k}}\left[2c^2T^2\dot{L} + cT\dot{V}\right] = \frac{\tilde{\beta}E'V^2}{2cL^3} \tag{B.16}$$

Now, as we have already seen, $\dot{V} = c\left[T\dot{L} + L\dot{T}\right]$. To make simple analytical progress, we follow Spence and Turcotte (1985) by looking for power law solutions where $T = hL^m$, where h and m are constants. This yields $L\dot{T} = mT\dot{L}$ and thus $\dot{V} = c(m+1)T\dot{L}$ such that (B.16) becomes

$$\frac{(3+m)c^2T^2L}{12\tilde{k}}\dot{L} = \frac{\tilde{\beta}E'V^2}{2cL^3}$$

(B.17)

Substituting for $\tilde{k} = d.\frac{(cT)^3}{12\mu}$ and $T = \frac{V}{cL}$ we get

$$\dot{L} = \frac{d\tilde{\beta}E'V^3}{2c(3+m)\mu L^5} \tag{B.18}$$

Rearranging and integrating over time gives

$$L(t) = A\left(\frac{E'S}{\eta}\right)^{\frac{1}{6}} \tag{B.19}$$

where the pre-factor $A = \left(\frac{3d\tilde{\beta}}{4c(3+m)}\right)^{\frac{1}{6}}$ and we have introduced the variable

$$S(t) = 4\int_0^t V(t)^3 dt \tag{B.20}$$

The pre-factor is calibrated using the linear growth case of $V = Qt$ examined by Spence and Turcotte (1985) for which $m = \frac{1}{2}$ and $A = 1.38$.

General solution

We determine how the length, maximum thickness and maximum pressure in the dike evolve over time from (B.19) for a general volumetric time evolution $V(t)$ as

$$L(t) = 1.38\left(\frac{E'S}{\eta}\right)^{\frac{1}{6}} \qquad T(t) = 1.38V\left(\frac{\eta}{E'S}\right)^{\frac{1}{6}} \qquad P(t) = 0.94V\left(\frac{E'^2\eta}{S}\right)^{\frac{1}{3}} \tag{B.21}$$

This assumes a self-similar shape for the dike during growth, although this will not necessarily be completely true during the relaxation phase, which is complicated by freezing.

Inflation stage solution for power law magma injection

If we assume power law growth during the inflation phase, such that $V(t) = Qt^s$, then (B.21) can be expressed as

$$L(t) = 1.38Q^{\frac{1}{2}}\left(\frac{\hat{\beta}E'}{\eta}\right)^{\frac{1}{6}} t^{\frac{3s+1}{6}} \qquad T(t) = 1.38Q^{\frac{1}{2}}\left(\frac{\eta}{\hat{\beta}E'}\right)^{\frac{1}{6}} t^{\frac{3s-1}{6}} \qquad P(t) = 0.94\left(\frac{E'^2\eta}{\hat{\beta}}\right)^{\frac{1}{3}} t^{-\frac{1}{3}} \tag{B.22}$$

where $\hat{\beta} = \frac{4}{3s+1}$. Note that the scaling is identical to the exact solution of Spence and Sharp (1985). Now, the thickness–length relationship can be written in a more general form as

$$T = 1.38^{1-m}\left(\frac{\eta}{\hat{\beta}E'}\right)^{\frac{1+m}{6}} L^m \tag{B.23}$$

where $m = \frac{3s-1}{3s+1}$. Note that Equation 6 is recovered if $s = 1$ when the exponent reduces to $m = \frac{1}{2}$.

Relaxation stage solution

If we assume growth ends at time $t = t_0$ then the final magma volume is $V(t_0) = V_0 = Qt_0^s$. The dike can still evolve over time even without magma emplacement, although at a much-reduced rate. If this evolution occurs for an additional relaxation time t_r such that $t = t_0 + t_r$, then from (B.20) we have

$$S = 4V_0^3\left(t_r + \frac{t_0}{3s+1}\right) \tag{B.24}$$

in (B.21). We can see that during volumetric growth the length increases as $t^{\frac{1}{6}+\frac{s}{2}}$ but during constant volume relaxation it increases more slowly, tending towards $t^{\frac{1}{6}}$ when $t_r \gg t_0$. Similarly, the thickness increases during volumetric growth as $t^{-\frac{1}{6}+\frac{s}{2}}$ and decreases during constant volume relaxation, tending towards $t^{-\frac{1}{6}}$ when $t_r \gg t_0$.

C. Solidification time

An upper estimate for the time for relaxation (before freezing) is obtained from equation (9)

$$t_r = \frac{T(t_r)^2}{16\kappa\beta^2} \tag{C.1}$$

where the final thickness $T(t_r)$ is given by (B.21) and (B.24). These equations can be re-arranged into a quartic in t_r

$$t_r^3\left(t_r+\frac{t_0}{3s+1}\right)=\frac{1.38^6V_0^3}{4(16\kappa\beta^2)^3}\left(\frac{\eta}{E'}\right) \tag{C.2}$$

which can be solved numerically.

References

A.C.F. Cocks, S.P.A. Gill, J. Pan (1998). "Modeling microstructure evolution in engineering materials", Advances in Applied Mechanics 36, 81-162.

A.M. Rubin (1995). "Propagation of magma filled cracks", Annu. Rev. Earth Planet. Sci. 23:287-336

D. A. Spence and P. Sharp (1985), "Self-Similar Solutions for Elastohydrodynamic Cavity Flow", Proceedings of the Royal Society of London. Series A, Mathematical and Physical Sciences , Aug. 8, 1985, Vol. 400, No. 1819, pp. 289-313.

D. A. Spence And D. L. Turcotte (1985), "Magma-Driven Propagation of Cracks", Journal Of Geophysical Research, Vol. 90, No. B1, Pages 575-580.